PROCEEDINGS OF ECOS 2023 - THE 36TH INTERNATIONAL CONFERENCE ON
EFFICIENCY, COST, OPTIMIZATION, SIMULATION AND ENVIRONMENTAL IMPACT OF ENERGY SYSTEMS
25-30 JUNE 2023, LAS PALMAS DE GRAN CANARIA, SPAIN

Performance characterization of the proton exchange membrane fuel cell (PEMFC) using the Lattice Boltzmann Modeling (LBM)

Hossein Pourrahmani[a], Milad Hosseini[b], Majid Siavashi[c], Hamza Moussaoui[d], Isabel Vázquez-Fernández[e], Mardit Matian[f], and Jan Van herle[g]

[a] Group of Energy Materials, École Polytechnique Fédérale de Lausanne (EPFL), Sion 1951, Switzerland, hossein.pourrahmani@epfl.ch, CA
[b] Applied Multiphase Fluid Dynamics Laboratory, School of Mechanical Engineering, Iran University of Science and Technology (IUST), Tehran, Iran, mldhosseini73@gmail.com
[c] Applied Multiphase Fluid Dynamics Laboratory, School of Mechanical Engineering, Iran University of Science and Technology (IUST), Tehran, Iran, msiavashi@iust.ac.ir
[d] Group of Energy Materials, École Polytechnique Fédérale de Lausanne (EPFL), Sion 1951, Switzerland, hamza.moussaoui@epfl.ch
[e] EH group, Chemin de Vuarpillière 27, Nyon 1260, Switzerland, isabel.vazquez@ehgroup.ch
[f] EH group, Chemin de Vuarpillière 27, Nyon 1260, Switzerland, mardit.matian@ehgroup.ch
[g] Group of Energy Materials, École Polytechnique Fédérale de Lausanne (EPFL), Sion 1951, Switzerland, jan.vanherle@epfl.ch

Abstract:

Fuel cells have proved to be promising alternatives for Internal Combustion Engines (ICEs) with higher efficiency and lower harmful environmental impact. Among different types, Proton Exchange Membrane Fuel Cell (PEMFC) has proved to be the best option to reach zero adverse emissions at low temperatures, which enables the operation of the PEMFC for mobility applications. However, cost, durability, and thermal/water management should be further considered to better commercialize PEMFCs. Durability and water/thermal management of the PEMFC can be improved by increasing the liquid removal from the gas diffusion layers (GDL) inside each stack of the PEMFC. However, there are no efficient simulation methods to analyze water removal based on experimental efforts. The goal of this study is to use the Lattice Boltzmann Method (LBM) to precisely capture the characterization of the GDLs that have been scanned by the Computed Tomography (CT) scans. Once the three-dimensional CT scans of the GDL are performed, the segmentation and reconstruction will be made to provide the needed geometry for fluid flow simulation. The geometry will be then used to characterize the effective parameters of the thermal/water management of the PEMFC. This study can also be a valid reference for future computational fluid dynamic analyses in the GDL using the numerical modeling with the conservative equations or the Lattice Boltzmann modeling (LBM) with the kinetic and particle distribution equations.

Keywords:

Proton exchange membrane fuel cell (PEMFC); Gas Diffusion layer (GDL); Lattice Boltzmann Method (LBM); Computed Tomography (CT) scan.

1. Introduction

The harmful environmental impacts of fossil fuels and the low efficiency of combustion engines have motivated the decision-makers to find alternative fuels [1]. In this regard, methanol, ethanol, bio-fuels, ammonia, hydrogen, etc. have been suggested as possible candidates having advantages/disadvantages for each of them [2]. Among the mentioned alternative fuels, hydrogen has been suggested as the most promising option for a wider spectrum of usages [3]. This means that hydrogen production methodologies should be developed to provide the required demand of fuel for different industries [4].

As a promising technology to facilitate the transition from fossil fuels to hydrogen, fuel cells are proposed [5]. Among the introduced fuel cell variants, the Proton Exchange Membrane Fuel Cell (PEMFC) is considered the most commercialized and efficient type in low-temperature operations [6]. The basis of PEMFC's operation is to use hydrogen as fuel and produce water and electricity as outputs [7]. Although significant developments have been achieved to improve the performance of the PEMFCs, the main barriers toward further commercialization of the PEMFCs are water/thermal management, cost, and durability [8].

https://doi.org/10.52202/069564-0038

Considering the low-temperature operation of the PEMFCs, a concentrated effort should be made to keep the operating conditions such as humidity and temperature in the desired range to manage the highest lifetime [9]. The PEMFC is a composition of different layers, namely, membrane, Catalyst Layer (CL), Gas Diffusion Layer (GDL), Micro-Porous Layer (MPL), and Bipolar Plate (BP) [10]. The desired operating temperature range of the membrane should be around 65 to 85 degrees Celsius to prevent drying or flooding the cell in addition to a humid condition to prevent drying the membrane [11]. However, high humidity results in the formation of water droplets/columns in the GDL, which acts as a diffusing medium to split the hydrogen and a backing layer to support the CL [12]. To improve water management and reduce the water columns (breakthroughs) inside the GDL, the MPL is being used [13]. The remaining water droplets in the GDL and MPL result in filling the pores and difficulties in cold start, that is starting the PEMFC from sub-zero temperatures [14]. In addition to the usage of MPL, controlling the capillary pressure in those regions are proven efficient method to prevent the formation of breakthroughs [15]. To control the capillary pressure, the microstructure and the wettability of the porous regions can be modified [16]. In other words, water management and the formation of breakthroughs in the GDL can be improved by the changes in the microstructure of the GDL [17]. Although these concepts are supported by the I-V characteristic curves and the experimental setups, novel simulation methods based on experiments should be developed to facilitate the quantitative measurements of each GDL's breakthroughs.

Although experimental methods are unable to calculate the number of each GDL's breakthroughs, the computational fluid dynamic (CFD) is able to present quantitative amounts in different applications [18]. The significant developments of the CFD commercial softwares such as ANSYS, and COMSOL have enabled the researchers to have a better vision of the fluid flow inside the porous media [19]. However, these softwares are developed based on conservation equations such as mass, energy, and momentum. This means that this commercial softwares cannot be used to simulate the fluid flow inside the GDL/MPL since the dominating driving force in those regions is the capillary pressure [20]. In this regard, CFD models that are based on the kinetics of the particles, such as the Lattice Boltzmann Method (LBM), rather than the conservation equations should be used to characterize the fluid flow inside the GDL/MPL and to quantitatively measure the formation of the breakthroughs in these regions [21]. Although the structure of the GDL and MPL can be obtained using different prediction methods, the exact structure can be observed using novel microscopy and tomography techniques [22].

To obtain the exact structure of a porous region, it is common to either use Focused Ion Beam-Scanning Electron Microscopy (FIB-SEM) or Computational Tomography (CT) scans [23]. Although FIB-SEM is an efficient method to characterize the structure of the GDL/MPL, it is a destructive method and demands special procedures to embed the samples to minimize the destruction of the samples through microscope imaging [24]. Additionally, FIB-SEM imaging demands more operation time to detect the structure of the same porous regions in comparison to the CT scan. CT scans [25] are also non-destructive and they are the best options considering the thickness of the GDL which is approximately around 200 μm. FIB-SEM is capable of measuring up to the resolution of 3 nm while CT scans reach 1 μm. Concerning the mentioned information, the combination of CT scans, which produce the exact geometry of the GDL, accompanied by the LBM CFD simulation will enable the quantitative measurement of the amount of water breakthroughs inside the GDL.

This study aims to provide a methodology to calculate the amount of water breakthroughs in an arbitrary GDL. The suggested methodology is based on using CT scan imaging to segment and reconstruct the exact geometry of the GDL in the PEMFCs. The reconstruction of the GDL provides the exact geometry of the GDL to be used for CFD simulations. This study benefits from LBM concepts, which are based on the kinetics of the particles rather than conservation principles in the CFD commercial softwares. The novelty of this study is to perform the quantitative measurement and characterization of the breakthroughs inside an arbitrary GDL using the LBM and CT scans. The results of this study can be used as a reference methodology to analyze the characteristics of the GDL considering the water/thermal management.

2. Problem description

This study aims at providing a reference method to characterize the water management of GDLs in PEMFC applications. In this regard, an arbitrary GDL sample has been used followed by the required CT scan to obtain the precise geometry of the carbon fibers for simulation purposes.

Figure 1 (a) shows the whole domain of the considered GDL sample while Figure 1 (b) illustrates the carbon fibers with more details. The mentioned geometry in Figure 1 has been obtained using $\mu - CT$ scan imaging with the operating conditions indicated in Table 1. The size of the sample is $1.685 \times 1.464 \times 0.225$ (mm^3) and the image resolution is 1 μm. The segmentation and reconstruction of the images have been done using Dragonfly software, Version 2020.2 developed by Object Research Systems (ORS) Inc in Montreal (Canada).

Once the segmentation and reconstruction of the GDL images are done, the reconstructed model was used to perform the Lattice Boltzmann Method (LBM) simulation to analyze the water flow in the GDL. The required governing equations to develop the LBM simulation model are presented in Section 3.. The results of the LBM

https://doi.org/10.52202/069564-0038

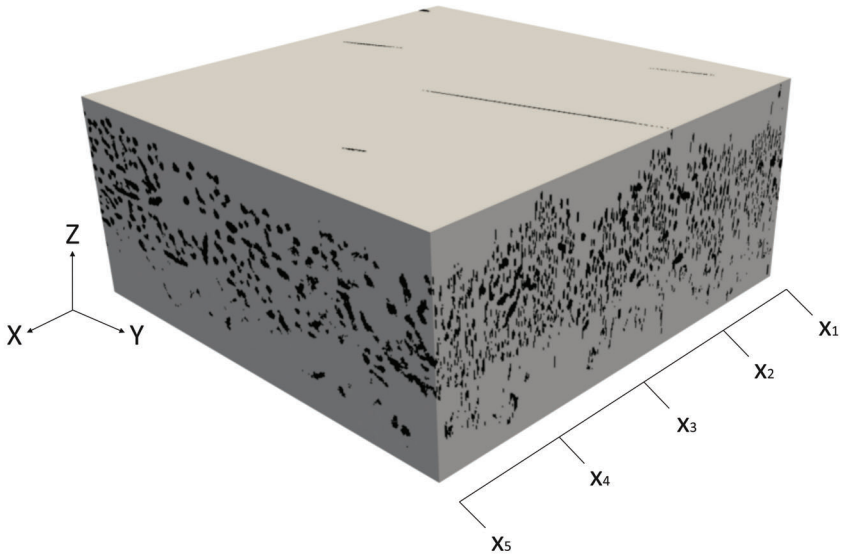

(a)

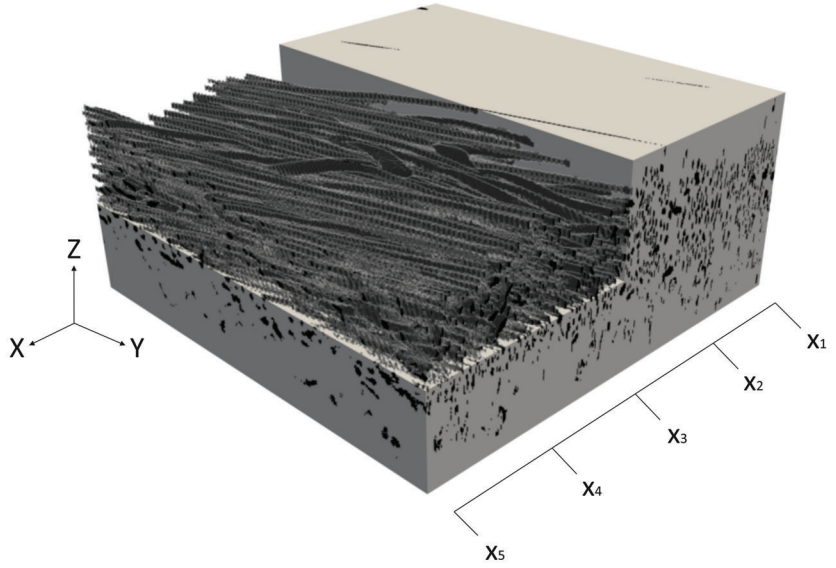

(b)

Figure 1: The schematic of the scanned, segmented, and reconstructed GDL to be analyzed using the LBM: (a) the whole considered region, (b) the clipped image to show the GDL inside the boundary condition.

simulation provide the three-dimensional flow distribution of the flow inside the GDL, hence the existence of breakthroughs (water columns) in the GDL can be predicted. It is believed that the formation of the water columns in the GDL is a form of degradation that fills the GDL pores and increases the possibility of remaining the water at sub-zero temperatures, leading to difficulties for the cold-start.

3. Governing equations

To implement the Multiple Relaxation-Time (MRT) model of the Lattice Boltzmann Method (LBM), the LBM can be developed based on the MRT collosion equation considering the force term as of Eq. 1 [26]:

Table 1: The operating conditions to perform the CT scans and the characteristics of the analyzed GDL sample

Parameter	Value	Parameter	Value
Acceleration voltage	40 kV	Averaging frames	10
Current	120 μA	Exposure time	500 ms
Image resolution	1 μm	Rotation step	0.22 degrees
Sample size (X-direction)	1.685 mm	Sample size (Y-direction)	1.464 mm
Sample size (Z-direction)	0.225 mm	Stage temperature	21 Celsius degrees
Voxel size (X-direction)	1685	Voxel size (Y-direction)	1464
Voxel size (Z-direction)	225		

$$f(x + e\Delta t, t + \Delta t) = f(x, t) - M^{-1}[SM(f^{eq}(x, t) - f(x, t)) + (I - \frac{1}{2}S)MF] \quad (1)$$

here, the density distribution function is shown with f (see Eq. 2 while Δt is the time step. M indicates the orthogonal matrix [27], which transfers the distribution functions and S is the diagonal matrix designed for D3Q19 as $S = \omega I$ [28]. As required in LBM, the discretized velocity is obtained using a D3Q19 lattice model, which is shown by e [29].

$$f_i^{eq}(\rho, u) = \rho w_i[1 + \frac{e_i.u}{c_s^2} + \frac{(e_i.u)^2}{2c_s^4} - \frac{u^2}{2c_s^2}] \quad (2)$$

where, F represents the body forces based on the Guo's model [30,31]:

$$F_i = \omega_i(\frac{e_i - u}{c_s^2} + \frac{(e_i.u)e_i}{c_s^4}).F \quad (3)$$

The indicated sound speed, c_s in 3 is considered to be $\frac{1}{\sqrt{3}}$. Each velocity direction is attributed with a weighting factor of ω_i based on ref. [26]. The respective values of the density and velocity can be obtained in Eqs. 4 and 5:

$$\rho = \Sigma_i f_i \quad (4)$$

$$u = \frac{1}{\rho}\Sigma_i e_i f_i + \frac{F\Delta t}{2\rho} \quad (5)$$

3.1. The magic parameter

Although in the Single Relaxation Time (SRT) LBM, the impacts of magic parameter is negligible on the results due to not being a parameter of viscosity, the MRT-LBM model demands the determination of magic parameter. For instance, the magic parameter can be calculated using Eq. 6 for Two Relaxation Time (TRT) LBM model:

$$\Lambda = \Lambda^+\Lambda^- = (\frac{1}{\omega^+\Delta t} - \frac{1}{2})(\frac{1}{\omega^-\Delta t} - \frac{1}{2}) \quad (6)$$

where, ω^- can be selected arbitrary while ω^+ should be computed through Eq. 7:

$$\vartheta = c_s^2(\frac{1}{\omega^+} - \frac{1}{2}) \quad (7)$$

In the MRT model, multiple frequencies correspond to the relaxation times and can be divided into symmetric, Λ_j^+, and anti-symmetric, Λ_k^-, groups. The combination of the mentioned two groups creates a single magic parameter that modifies the simulation error as follows [32]:

$$\Lambda_{j,k} = \Lambda_j^+\Lambda_k^- j = e, \pi, \varepsilon, \vartheta k = q, m \quad (8)$$

$$\Lambda_{j,k} = [\Lambda_\vartheta^+\Lambda_q^-, \Lambda_e^+\Lambda_q^-, \Lambda_\varepsilon^+\Lambda_q^-, \Lambda_\pi^+\Lambda_q^-, \Lambda_\vartheta^+\Lambda_m^-, \Lambda_e^+\Lambda_m^-, \Lambda_\varepsilon^+\Lambda_m^-, \Lambda_\pi^+\Lambda_m^-] \quad (9)$$

Considering the 9, there are eight different magic parameters for the D3Q19 model. As all the magic parameters are considered identical, the presented MRT can be assumed as TRT model. Thus, the existing frequencies of the symmetric group ω^s can be considered equal to the calculated frequency from the viscosity as of Eq. 10:

$$\omega^s = \frac{1}{\frac{\vartheta}{c_s^2\Delta t} + \frac{1}{2}} \quad (10)$$

https://doi.org/10.52202/069564-0038

where, the superscript "*s*" indicates the existing frequencies of the symmetric part. the related superscript for the anti-symmetric part is "*as*" and the corresponding frequency can be calculated using Eq. 11:

$$\omega^{as} = \frac{4 - 2\omega^{s}}{(4\Lambda - 1)\omega^{s} + 2} \tag{11}$$

3.2. Mean velocity computation

Considering the Darcy model, the permeability tensor is defined as follows:

$$K_{ij} = \frac{\mu}{\Delta P_j}\bar{U}_i; i, j = 1, 2, 3 \tag{12}$$

here, ΔP_j is the pressure gradient in j-direction while $\bar{U}_i$ is the mean volumetric velocity in the i-direction as follows [33]:

$$\bar{U}_i = \frac{1}{V_t}\int_{\Omega} u_i d\Omega \tag{13}$$

where, V_t is the total volume of the sample while $d\Omega$ is the volumetric element in the pore domain. Using the trapezoidal discrete form, Eq. 14 can be solved as follows:

$$\bar{U}_x = \frac{\Sigma_k^{N_k}\Sigma_j^{N_j}\Sigma_i^{N_i} u_{x_{ijk}}}{N_i N_j N_k} \tag{14}$$

Accounting the form of Eq. 14, error will be produced, which can be controlled using the magic parameter, and by using high-order interpolations to solve the Eq. 13. The effective permeability can be presented as follows [34]:

$$K_{eff} = K_{ideal} + \frac{2}{3}\Lambda - \frac{1}{12} \tag{15}$$

where, K_{ideal} is the exact value of the permeability in the ideal boundary condition.

4. Results and discussion

In the first step, the GDL sample, shown in Figure 1, is scanned with $\mu - CT$ imaging to enable the segmentation and reconstruction of the sample for CFD analysis. Furthermore, the $\mu - CT$ imaging enables the calculation of the porosity and the mean pore diameter that can be needed for the LBM simulation. Using the Dragonfly software and after the reconstruction of the images, the respective values of the porosity and the mean pore diameter were calculated to be 0.8516 and 2.894 μm, respectively.

As mentioned in Section 3., there are three methods to use the LBM, Single-Relaxation Times (SRT), Two-Relaxation Times (TRT), or Multi-Relaxation Time (MRT). Among these methods, the MRT-LBM benefits from the highest accuracy and precision, hence this study has utilized this model to simulate the scanned GDL sample by the $\mu - CT$ imaging. Each of the Lattice vectors is located in the position of x and the time of t, which enables the transient simulation of the fluid flow inside the GDL. In this study, the D3Q19 discretization model has been used, that means each of the lattice vectors has 19 different components in the momentum space.

Accounting for the boundary conditions, the fluid flow is at low speeds (laminar flow) and Darcy conditions and the aim is to consider the capillary pressure as well. The implemented pressure gradient as the driving force for the fluid flow in the Z-direction, shown in Figure 1, is 0.1 $\frac{Pa}{m}$. The four surfaces of the GDL sample shown in Figure 1 parallel to the ZY and XZ planes are considered walls with no-slip boundary conditions.

A simplification has been made and pure water has been selected for the working fluid. In this regard, the kinematic viscosity of the fluid is 0.802 $\frac{mm^2}{s}$ while the fluid density is 995.7 $\frac{kg}{m^3}$. The maximum number of iterations for flow simulation is 80,000,000 while the Navier-Stokes relaxation time is 1. Additionally, the frequency that the convergence being checked is 0.5 s while the convergence criteria for the flow field is 10^{-4}. The inflation parameter regarding the LBM simulation, which considers the surface mesh before the visualization is 0.1.

Once the required parameters for the LBM simulation are provided, the fluid flow analysis is done. Figure 2 presents the results of the LBM simulation for the GDL sample shown in Figure 1. As can be seen, there are regions with higher velocities in the three-dimensional domain with red, yellow, and green colors. These regions are indicators of the possibilities for the formation of breakthroughs inside the GDL. Notably, the analyzed GDL by the $\mu - CT$ scan has not gone through aging and is a pristine sample. To have a better visualization of the breakthroughs inside the GDL, Figure 3 is provided, which illustrates the fluid flow inside the GDL considering

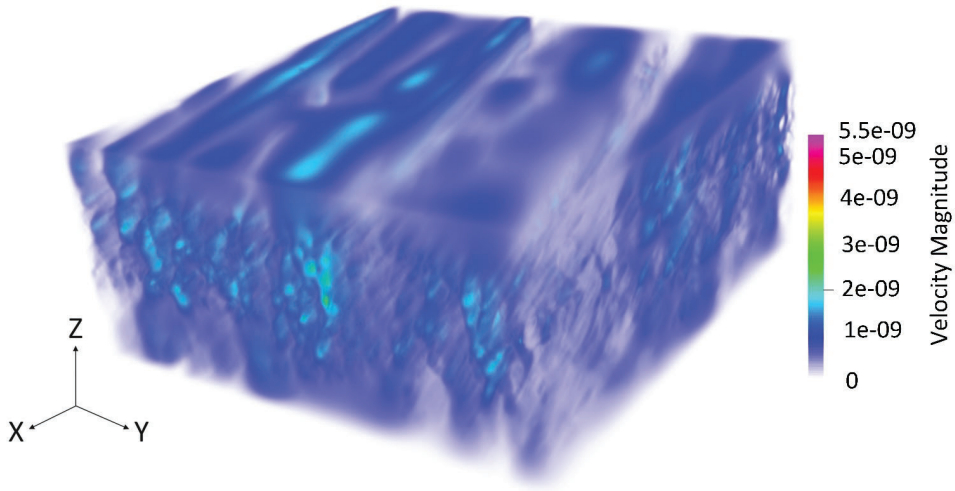

(a)

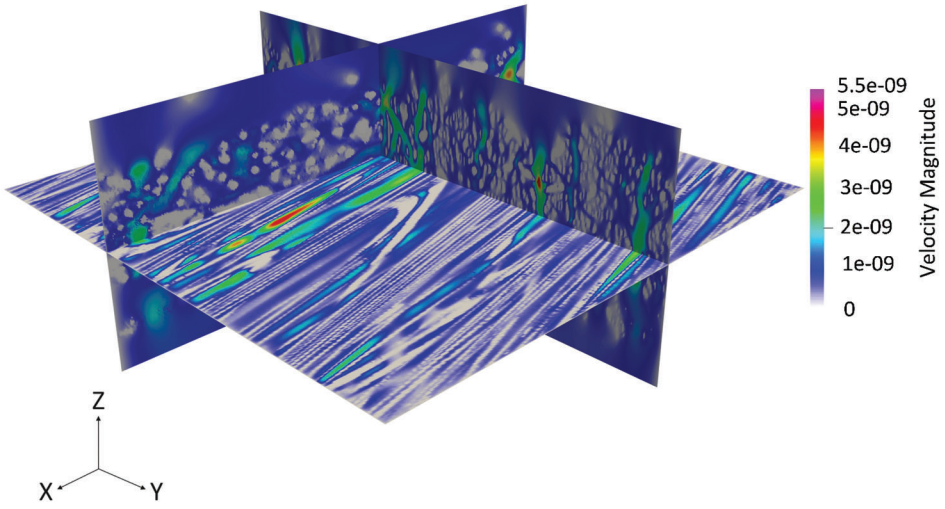

(b)

Figure 2: The three-dimensional results of the performed CFD analysis using the LBM method on the presented sample in Figure 1: (a) The three-dimensional changes in the velocity in the considered domain, (b) The changes in the velocity considering three different slices in the X-, Y-, and Z- directions.

the X_1, X_2, X_3, X_4, and X_5 slices shown in Figure 1. Specifically, in Figure 3(c) and 3(e), the breakthroughs can be seen, as the green regions (indicating the breakthrough) pass through the GDL carbon fibers. The GDL carbon fibers in Figure 3 are shown with while values since the velocity vectors are zero if there exist solid materials.

As Figure 2 illustrates, the visualization of the breakthroughs inside the GDL is not a straightforward procedure and better quantification measurements are required. In this regard, each voxel that has velocity values of more than 2×10^{-9} in the domain given by Figure 2 (a) is considered as a region of breakthrough. In this regard, 9.13% of the GDL porous region, which is illustrated in Figure 2(a), is consisted of the breakthroughs. This means that 50,675,060 voxels are labeled as breakthroughs inside the whole domain with 555,039,000 voxels. In other words, 0.051 mm^3 of the illustrated domain in Figure 1 is prone to create breakthroughs in the whole domain of 0.555 mm^3.

https://doi.org/10.52202/069564-0038

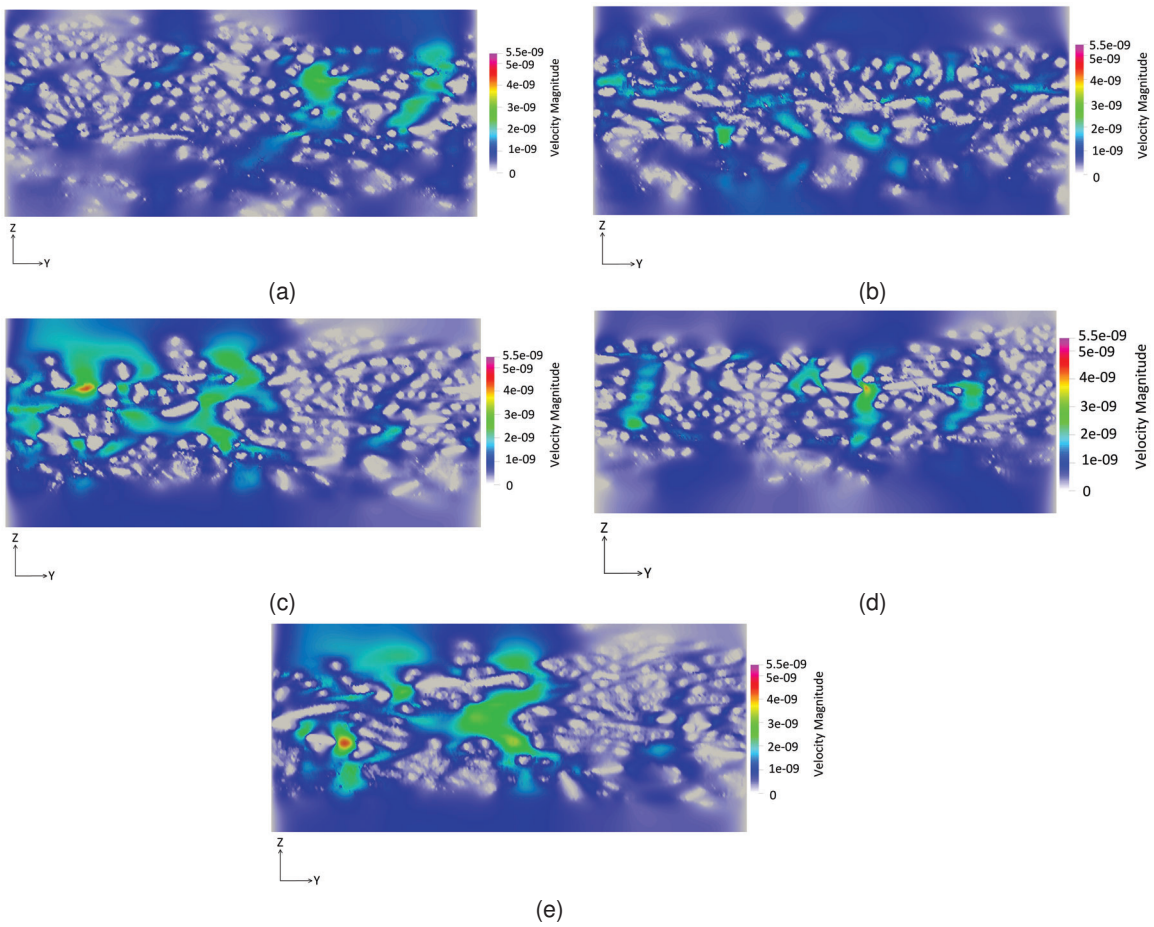

Figure 3: The two-dimensional velocity contours in the X-direction after performing the LBM simulations on the analyzed samples shown in Figure 1: (a) Slice X_1 depicted in Figure 1, (b) Slice X_2 depicted in Figure 1, (c) Slice X_3 depicted in Figure 1, (d) Slice X_4 depicted in Figure 1, (e) Slice X_5 depicted in Figure 1

5. Conclusion

This study could analyze the formation of the water columns inside the GDL of the PEMFC. The formation of water columns, which is also famous as breakthroughs, is known as a degradation phenomenon that fills the pores and leads to difficulties in starting the cell from sub-zero temperatures. As the driving force of the fluid flow in the GDL is the capillary pressure, the conventional conservation principles such as momentum, energy, and mass are not the governing equations, and methods based on the kinetics of the particles should be used. In this regard, LBM formulation, which is considered a powerful CFD methodology based on the kinetics of the particles to simulate the fluid flow at the interfaces between the gas/solid/liquid and at low-velocity conditions, has been used using the obtained $\mu - CT$ images of the GDL. $\mu - CT$ images could provide the exact geometry of the GDL followed by the porosity and the mean pore diameter that is required for the LBM simulation.

The results of the LBM simulation could provide the velocities of the water passing through the GDL. The illustrated contours visualized the locations of the breakthroughs followed by the corresponding voxels. To enable the quantitative measurement of the breakthroughs, the voxels with higher velocity values of 2×10^{-9} were considered to be a part of the breakthroughs in the domain. In this regard, it was calculated that 50,675,060 voxels are labeled as breakthroughs among the whole 555,039,000 voxels. In other words, considering the whole size of the domain, which is 0.555 mm^3, the created breakthrough is equal to 0.051 mm^3. The LBM simulation could also provide a quantitative percentage of 9.13% as the share of the breakthrough in the whole domain.

The output results of this study proved that the performance of the GDLs can be characterized without experimental testing and novel GDLs can be analyzed before assembly to reduce the costs and time. The current novelty of this study can be used in future studies to facilitate GDL characterization. Additionally, the following

topics can be accounted for future studies:

- This study only analyzed an arbitrary pristine GDL to analyze the possibility of the GDL characterization using the LBM simulation and CT scan imaging. It is suggested to consider aged or degraded samples of GDL and evaluate the impacts of different types of degradation phenomena on the amount of created breakthroughs.
- To facilitate the LBM simulations, simplifications were made and only pure water was considered as the fluid flow in the GDL. However, in reality, the fluid is either hydrogen or oxygen in a humid environment with the possibility of water formation.
- LBM simulation is also a powerful tool to analyze the droplet formation and movement in porous media, which is the exact electrochemical phenomenon inside the GDL. In this regard, further details can be added to this model to obtain the highest precision in the simulation results.

Acknowledgments

This project has received funding from the European Union's Horizon 2020 research and innovation program under the Marie Sklodowska-Curie grant agreement No. 754354.

The segmentation and reconstruction of the images have been done using the Dragonfly software, Version 2020.2 developed by Object Research Systems (ORS) Inc in Montreal, Canada. The required link to the company's website is: http://www.theobjects.com/dragonfly.

References

[1] H. Pourrahmani *et al.*, "Water management of the proton exchange membrane fuel cells: Optimizing the effect of microstructural properties on the gas diffusion layer liquid removal," *Energy*, vol. 256, p. 124712, 2022.

[2] H. Pourrahmani, M. Gay, A. Yavarinasab *et al.*, "Optimization and dynamic responses of an integrated fuel cell and battery system for an 800 kw ferry: A case study," *Energy Reports*, vol. 8, pp. 9757–9776, 2022.

[3] M. Gay, H. Pourrahmani *et al.*, "Fuel cell and battery technologies for a 800 kw ferry: Two optimized scenarios," *Science Talks*, vol. 3, p. 100039, 2022.

[4] V. Walter, L. Göransson, M. Taljegard, S. Öberg, and M. Odenberger, "Low-cost hydrogen in the future european electricity system–enabled by flexibility in time and space," *Applied Energy*, vol. 330, p. 120315, 2023.

[5] H. Pourrahmani, C. Xu, and J. Van herle, "Two novel cogeneration charging stations for electric vehicles: Energy, exergy, economic, environment, and dynamic characterizations," *Energy Conversion and Management*, vol. 271, p. 116314, 2022.

[6] H. Pourrahmani, A. Rajabi *et al.*, "A modified design of the gas flow channel geometry for the proton exchange membrane fuel cells: A three-dimensional simulation," *Science Talks*, vol. 3, 2022.

[7] H. Pourrahmani and J. Van herle, "Evaluation criterion of proton exchange membrane (ecpem) fuel cells considering inserted porous media inside the gas flow channel," *Applied Thermal Engineering*, vol. 203, p. 117952, 2022.

[8] Y. Wang, D. F. R. Diaz, K. S. Chen, Z. Wang, and X. C. Adroher, "Materials, technological status, and fundamentals of pem fuel cells–a review," *Materials today*, vol. 32, pp. 178–203, 2020.

[9] M. Raeesi, S. Changizian, P. Ahmadi, and A. Khoshnevisan, "Performance analysis of a degraded pem fuel cell stack for hydrogen passenger vehicles based on machine learning algorithms in real driving conditions," *Energy Conversion and Management*, vol. 248, p. 114793, 2021.

[10] K. Christmann, K. A. Friedrich, and N. Zamel, "Activation mechanisms in the catalyst coated membrane of pem fuel cells," *Progress in Energy and Combustion Science*, vol. 85, p. 100924, 2021.

[11] L. Xu, Z. Hu, C. Fang, J. Li, P. Hong, H. Jiang, D. Guo, and M. Ouyang, "Anode state observation of polymer electrolyte membrane fuel cell based on unscented kalman filter and relative humidity sensor before flooding," *Renewable Energy*, vol. 168, pp. 1294–1307, 2021.

[12] M. Mortazavi, A. D. Santamaria, V. Chauhan, J. Z. Benner, M. Heidari, and E. F. Médici, "Effect of pem fuel cell porous media compression on in-plane transport phenomena," *Journal of Power Sources Advances*, vol. 1, p. 100001, 2020.

https://doi.org/10.52202/069564-0038

[13] F. S. Nanadegani, E. N. Lay, and B. Sunden, “Effects of an mpl on water and thermal management in a pemfc,” *International Journal of Energy Research*, vol. 43, no. 1, pp. 274–296, 2019.

[14] W. Pan, P. Li, Q. Gan, X. Chen, F. Wang, and G. Dai, “Thermal stability analysis of cold start processes in pem fuel cells,” *Applied Energy*, vol. 261, p. 114430, 2020.

[15] D. Niblett, V. Niasar, S. Holmes, A. Mularczyk, J. Eller, R. Prosser, and M. Mamlouk, “Water cluster characteristics of fuel cell gas diffusion layers with artificial microporous layer crack dilation,” *Journal of Power Sources*, vol. 555, p. 232383, 2023.

[16] H. Pourrahmani and J. Van herle, “The impacts of the gas diffusion layer contact angle on the water management of the proton exchange membrane fuel cells: Three-dimensional simulation and optimization,” *International Journal of Energy Research*, vol. 46, no. 11, pp. 16 027–16 040, 2022.

[17] D. Zapardiel and P. A. García-Salaberri, “Modeling the interplay between water capillary transport and species diffusion in gas diffusion layers of proton exchange fuel cells using a hybrid computational fluid dynamics formulation,” *Journal of Power Sources*, vol. 520, p. 230735, 2022.

[18] Y. Zhang, S. He, X. Jiang, M. Xiong, Y. Ye, and X. Yang, “Three-dimensional multi-phase simulation of proton exchange membrane fuel cell performance considering constriction straight channel,” *Energy*, vol. 267, p. 126544, 2023.

[19] H. Pourrahmani, M. Moghimi, M. Siavashi, and M. Shirbani, “Sensitivity analysis and performance evaluation of the pemfc using wave-like porous ribs,” *Applied Thermal Engineering*, vol. 150, pp. 433–444, 2019.

[20] Y. Wang, H. Xu, W. He, Y. Zhao, and X. Wang, “Lattice boltzmann simulation of the structural degradation of a gas diffusion layer for a proton exchange membrane fuel cell,” *Journal of Power Sources*, vol. 556, p. 232452, 2023.

[21] P. Sarkezi-Selsky, H. Schmies, A. Kube, A. Latz, and T. Jahnke, “Lattice boltzmann simulation of liquid water transport in gas diffusion layers of proton exchange membrane fuel cells: Parametric studies on capillary hysteresis,” *Journal of Power Sources*, vol. 535, p. 231381, 2022.

[22] H. Pourrahmani, M. Matian, and J. Van Herle, “Poisoning effects of cerium oxide (ceo2) on the performance of proton exchange membrane fuel cells (pemfcs),” *ChemEngineering*, vol. 6, no. 3, p. 36, 2022.

[23] E. Leonard, A. D. Shum, N. Danilovic, C. Capuano, K. E. Ayers, L. M. Pant, A. Z. Weber, X. Xiao, D. Y. Parkinson, and I. V. Zenyuk, “Interfacial analysis of a pem electrolyzer using x-ray computed tomography,” *Sustainable Energy & Fuels*, vol. 4, no. 2, pp. 921–931, 2020.

[24] R. Moroni and S. Thiele, “Fib/sem tomography segmentation by optical flow estimation,” *Ultramicroscopy*, vol. 219, p. 113090, 2020.

[25] P. Irmscher, D. Qui, H. Janßen, W. Lehnert, and D. Stolten, “Impact of gas diffusion layer mechanics on pem fuel cell performance,” *International Journal of Hydrogen Energy*, vol. 44, no. 41, pp. 23 406–23 415, 2019.

[26] T. Krüger, H. Kusumaatmaja, A. Kuzmin, O. Shardt, G. Silva, and E. M. Viggen, “The lattice boltzmann method,” *Springer International Publishing*, vol. 10, no. 978-3, pp. 4–15, 2017.

[27] D. d’Humières, “Multiple–relaxation–time lattice boltzmann models in three dimensions,” *Philosophical Transactions of the Royal Society of London. Series A: Mathematical, Physical and Engineering Sciences*, vol. 360, no. 1792, pp. 437–451, 2002.

[28] I. Ginzburg, F. Verhaeghe, and D. d’Humieres, “Study of simple hydrodynamic solutions with the two-relaxation-times lattice boltzmann scheme,” *Communications in computational physics*, vol. 3, no. 3, pp. 519–581, 2008.

[29] M. Hosseini, M. Siavashi, M. Shirbani, and M. M. Nezhad, “Reliability assessment of the lattice-boltzmann method for modeling and quantification of hydrological attributes of porous media from microtomography images,” *Advances in Water Resources*, vol. 171, p. 104351, 2023.

[30] Z. Guo, C. Zheng, and B. Shi, “Discrete lattice effects on the forcing term in the lattice boltzmann method,” *Physical review E*, vol. 65, no. 4, p. 046308, 2002.

[31] G. Silva and V. Semiao, “First-and second-order forcing expansions in a lattice boltzmann method reproducing isothermal hydrodynamics in artificial compressibility form,” *Journal of fluid mechanics*, vol. 698, pp. 282–303, 2012.

[32] S. Khirevich and T. W. Patzek, “Behavior of numerical error in pore-scale lattice boltzmann simulations with simple bounce-back rule: Analysis and highly accurate extrapolation,” *Physics of Fluids*, vol. 30, no. 9, p. 093604, 2018.

[33] B. P. Muljadi, M. J. Blunt, A. Q. Raeini, and B. Bijeljic, “The impact of porous media heterogeneity on non-darcy flow behaviour from pore-scale simulation,” *Advances in water resources*, vol. 95, pp. 329–340, 2016.

[34] L. Talon, D. Bauer, N. Gland, S. Youssef, H. Auradou, and I. Ginzburg, “Assessment of the two relaxation time lattice-boltzmann scheme to simulate stokes flow in porous media,” *Water Resources Research*, vol. 48, no. 4, 2012.

https://doi.org/10.52202/069564-0038